International Journal of Fatigue 33 (2011) 300–312

Contents lists available at ScienceDirect

International Journal of Fatigue

journal homepage: www.elsevier.com/locate/ijfatigue

Fatigue testing and analysis of peened highway bridge welds under in-service variable amplitude loading conditions

Kasra Ghahremani, Scott Walbridge *

Department of Civil and Environmental Engineering, University of Waterloo, Ontario, Canada N2L 3G1

ARTICLE INFO

Article history:
Received 25 June 2010
Received in revised form 2 September 2010
Accepted 6 September 2010
Available online 21 September 2010

Keywords:
Fatigue
Fracture mechanics
Needle peening
Steel bridges
Variable amplitude loading

ABSTRACT

A laboratory study is presented wherein needle peened structural steel weld specimens are fatigue tested under simulated in-service loading histories typical of highway bridges. A strain-based fracture mechanics model is then validated by comparison with the test results and used to perform additional studies, wherein similar welds are analyzed under loading histories encompassing a wider range of influence lines and bridge spans. It is concluded that the employed model is well suited for studying the effects of peening on the fatigue performance of highway bridge welds under in-service loading conditions. The consideration of tensile dead load stresses and periodic overload trucks is seen to decrease the predicted benefit of peening. This benefit can still be substantial, however, for a wide range of loading conditions likely to be seen in highway bridges.

1. Introduction

The possible applications of peening treatments [1–12] for enhancing the fatigue performance of large welded steel structures are wide ranging and include: bridges, ships, offshore structures, wind turbines, cranes, and heavy mining equipment. Peening treatments can be applied to new structures to increase their design service life or reduce their self-weight. These treatments can also be applied to existing structures, in order to extend their service lives or increase their fatigue strengths in view of changing service requirements or detected deficiencies.

Peening treatments have been shown to improve the fatigue performance of welds primarily by introducing compressive residual stresses near the treated surface, which have the effect of reducing crack growth rates at the smaller crack depths [1,2]. In some cases, other peening effects may also contribute to the fatigue performance improvement, such as increasing the weld toe radius or the local hardness of the treated surface [3,4]. As a repair method for structures already containing large fatigue cracks (i.e. greater than the depth of the introduced compressive residual stress field), peening alone is generally ineffective. Peening can be used in conjunction with grinding and rewelding, however, as an effective means of repairing large fatigue cracks in existing structures. Possible negative effects of peening may include: roughening of the treated surface, the formation of cold laps that can act as crack initiation sites, and embrittlement of the treated surface. In general, however, it has been found that these effects are not significant when controlled, mild peening treatments are applied to weld toes, which tend to already possess initial defects, high tensile residual stresses, and a sharp local notch.

Significant empirical evidence can be found in the existing literature that peening treatments, such as shot, needle, and hammer peening and ultrasonic impact treatment (UIT), are effective in increasing the fatigue performance of welds under laboratory-controlled constant amplitude (CA) loading conditions (e.g. [1–7]). Much of this work has focused on tension-only loading. However, some studies have also looked at load ratio effects. To date, the number of studies examining the fatigue performance of peened welds under variable amplitude (VA) loading conditions is limited [8–12].

The fatigue behaviour of untreated plain and welded steel specimens under VA loading conditions is a research area that has received considerable recent attention (e.g. [13–15]) and continues to evolve as our understanding improves of the mechanisms that cause VA loading behaviour to differ from what might be expected, based on the results of CA loading tests.

In the research to date of peened welds subjected to VA loading conditions, it has been found that design methods shown to be effective in correlating CA and VA test data for untreated welds, can yield unsafe predictions when used to evaluate VA test data for peened welds [9]. There are several possible reasons for this.

* Corresponding author. Address: Department of Civil and Environmental Engineering, University of Waterloo, 200 University Avenue West, Waterloo, Ontario, Canada N2L 3G1. Tel.: +1 519 888 4567x38066; fax: +1 519 888 4349.
E-mail address: swalbrid@civmail.uwaterloo.ca (S. Walbridge).

0142-1123/$ - see front matter © 2010 Elsevier Ltd. All rights reserved.
doi:10.1016/j.ijfatigue.2010.09.004

Among the more concerning of these is the increased potential for crack growth rate changes or residual stress relaxation following "overload" events.

Under VA loading conditions, overload events can lead to accelerated crack growth in treated welds as a result of the following mechanisms: (1) compressive overloads (also known as "underloads") can cause relaxation of the compressive residual stresses introduced by the peening treatment if the total (residual + applied) stress is sufficient to cause a significant non-linear material response, and (2) compressive (as well as very large tensile) overloads can have the effect of reducing the crack opening stress level, and thus increasing the effective portion of the applied stress cycles, for a number of cycles following the overload event. These two mechanisms are illustrated in Fig. 1. Note that in Fig. 1a, σ_{res} is the local residual stress, $\sigma_{app,el}$ is the subsequently applied elastic local stress, and σ_{app} is the actual applied local stress. In Fig. 1b, the applied stress history consists of 10 underload cycles followed by 990 constant amplitude cycles. The thick dashed line in this figure shows the gradual build-up of the crack opening stress (σ_{op}) following the underload cycles.

In [12], a strain-based fracture mechanics (SBFM) model is used to analyze peened welds under loading histories consisting of blocks of tension-only cycles interspersed with periodic underload events. The primary advantage of this model is its inherent capability of predicting the two crack growth accelerating mechanisms described in Fig. 1. Under loading conditions expected to result in a primarily linear material response, the fatigue life improvement predictions are seen in [12] to converge on those obtained using linear elastic fracture mechanics (LEFM) models. The SBFM model's predictive capabilities in the current context are demonstrated in [12] by comparison with fatigue test results. The work in [12] is limited, however, to the investigation of idealized block loading histories. Herein, this work is extended to examination of the behaviour of peened welds under VA loading conditions more typical of highway bridges in-service.

In the following sections, the laboratory portion of this investigation is first summarized, including the fatigue testing of as-received and needle peened welds under two simulated in-service loading histories. Ancillary tests performed to determine various material and geometric parameters required for the fracture mechanics analysis, as well as the local residual stress and micro-hardness distributions along the anticipated crack path, are also described and the results summarized. Following this, an SBFM model is described and validated for analysis of peened welds by comparison with the test results. A number of analytical studies are then presented, wherein similar welds are analyzed under in-service loading histories encompassing a wider range of influence lines, bridge spans, and loading conditions. Based on these analyses, conclusions are drawn regarding the influence of the examined parameters on the fatigue performance enhancement that can be achieved by needle peening.

The presented research focuses on the investigation of needle peening. In comparison with other peening treatments such as shot and hammer peening and UIT, needle peening has a number of noteworthy advantages and disadvantages. As a pneumatic tool is used, rather than projectiles, it is considered to be superior to shot peening for field applications involving bridges. As the impacting needles are small in diameter in comparison with hammer peening and UIT indenters, it has the advantage that there is a better chance of the needles reaching the deepest part of the weld notch. It is a relatively mild treatment in comparison with hammer peening, meaning the introduced compressive residual stress field is not as deep. However this also means less plastic deformation, and thus, a reduced risk of surface embrittlement. In comparison with UIT, needle peening is considered to be inferior from an occupational health standpoint, as it produces much more noise and vibration. Needle peening has an advantage over UIT, however, of being relatively less expensive.

2. Laboratory test procedures

2.1. Fatigue tests of as-received and peened welds

The fatigue specimens used in this study were small-scale fatigue specimens consisting of a Detail Category 'C' [16,17] non-load carrying fillet welded attachment, representative of a typical transverse web stiffener in a bridge girder. In the first phase of the testing program, the specimens were constructed of 9.5 mm (3/8″) CSA 350 W [18] steel plate (mild structural steel with a 350 MPa nominal yield strength) and had a width of 30 mm. They were made by saw cutting slices from larger (300 mm wide) welded joints fabricated using the FCAW welding process (see Fig. 2a).

During testing, premature specimen failures through the base metal near the grips of the testing machine were observed for a number of the peened specimens under certain loading conditions. To avoid this in subsequent testing, a modified specimen geometry was developed, based on [19], with a wider (50 mm) gripping region, but the same 30 mm width retained at the weld location (see Fig. 2b). These specimens were fabricated by saw cutting 50 mm wide slices from 300 mm wide welded joints, and then cutting the final curved shape using a CNC machine.

Including the twelve tests reported in [12], a total of 50 fatigue tests were carried out on as-welded and peened specimens under different cyclic loading conditions (see Table 1). For each set of parameters, at least three tests were performed. The specimens

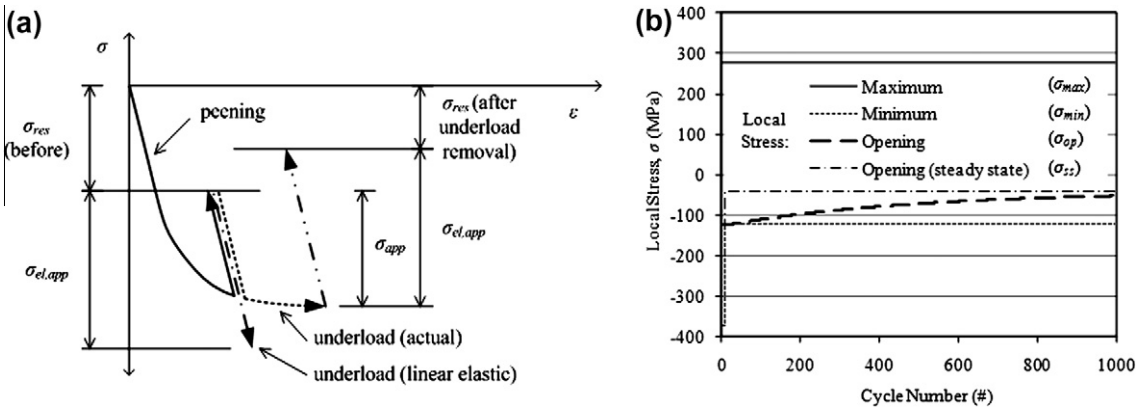

Fig. 1. Overload effects on local stresses for peened welds. (a) Residual stress relaxation. (b) Crack opening stress reduction [12].

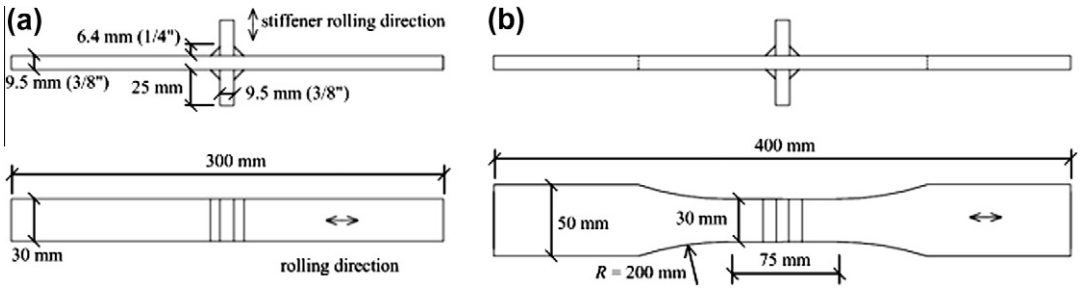

Fig. 2. Transverse stiffener specimen geometries. (a) Straight. (b) Variable width.

Table 1
Fatigue test program.

ΔS or ΔS_{eq} (MPa)	R (–)	Loading (–)	Treatment (–)	Specimens (#)
180	0.1	CA	AW	3[a]
180	0.1	CA	NP	3[a]
270	0.1	CA	AW	4
270	0.1	CA	NP	4
180	0.4	CA	AW	3
180	0.4	CA	NP	3
400	−1.0	CA	AW	3
400	−1.0	CA	NP	3
186	0.1	CA-UL	AW	3[a]
186	0.1	CA-UL	NP	3[a]
279	0.1	CA-UL	AW	3
279	0.1	CA-UL	NP	3
159	–	ps-m-40	AW	3
159	–	ps-m-40	NP	3
161	–	ps-r-15	AW	3
161	–	ps-r-15	NP	3

Note: AW = "as-welded", NP = "needle peened".
[a] Test results previously reported in [12].

assigned to each test set were selected randomly, but in such a way that all sets contained specimens each cut from different larger plates.

Four different types of fatigue loading were considered: constant amplitude (CA) loading, CA loading with periodic underloads (CA-UL), and two in-service variable amplitude (VA) loading histories. These different loading types are illustrated in Fig. 3. In addition to varying the loading type, the equivalent nominal stress ranges, ΔS_{eq}, and ratios, R, were varied in certain cases. The CA-UL history consisted of a 1000 cycle repeating block, whereas the two VA histories each consisted of 100 cycle repeating blocks. In the fatigue tests, the loading histories were imposed using sinusoidal load profiles with a loading frequency of 8 Hz [21]. All testing was performed at indoor ambient temperature (~21 °C) and humidity. Each loading block was repeated until either the specimen failed or roughly 3 million cycles were applied, at which point the test was considered a "runout".

The two VA spectrum blocks were randomly extracted from larger in-service loading histories. These histories were generated

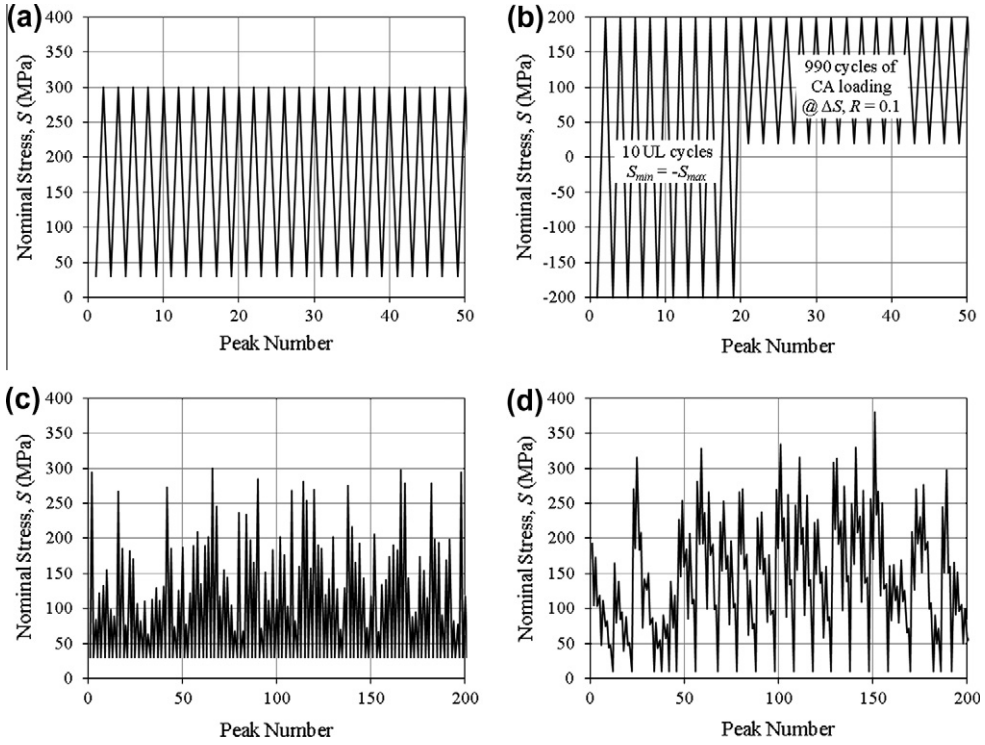

Fig. 3. Fatigue test loading types. (a) CA. (b) CA-UL. (c) VA: ps-m-40. (d) VA: ps-r-15.

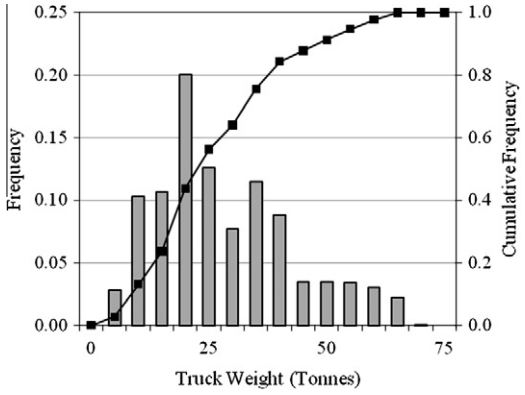

Fig. 4. Truck weight histogram based on 1995 Ontario survey [20].

using traffic data from Ontario, Canada obtained from a survey of axle spacings and loads conducted in 1995 [20], which included a total of 10,198 trucks. Fig. 4 shows a gross truck weight (GVW) histogram based on the survey data. To generate loading histories, the trucks were successively passed over influence lines for two locations on simply-supported bridge girders with different spans. Specifically, the following cases were considered: the mid-span moment of a 40 m girder (ps-m-40) and the support reaction of a 15 m girder (ps-r-15).

Comparing the two VA loading history segments, significant differences can be seen. The first segment (ps-m-40, Fig. 3c) can be characterized as being more narrow-banded. In this case, the passage of a truck over the bridge generally results in only a single large load cycle, since the bridge span is much longer than the truck length. In the second case (ps-r-15, Fig. 3d), each axle load tends to cause a small cycle as it comes on or off the end of the bridge.

The needle peening was performed using a compressed air needle gun with rounded needle ends, following the procedure recommended by the International Institute of Welding [22]. Each treated specimen was subjected to four peening passes lasting ~3 s each.

To monitor crack growth, visual inspection and the alternating current potential drop (ACPD) method were employed. The ACPD instrumentation consisted of a TSC Mk IV ACPD system, along with four custom probes that could be attached to the specimens magnetically and provided crack depth measurements at two locations (centred on the specimen and spaced 10 mm apart) on each of the weld toes (see Fig. 5). The ACPD system only became available part way through the testing program. Thus, crack growth measurements were not obtained for all of the tests. To evaluate the accuracy of the system, dye penetrant staining was used upon crack detection in three specimens and the actual crack depths were compared with the ACPD readings after complete specimen fracture.

2.2. Micro-hardness and residual stress measurements

To study the effect of peening on the near-surface hardness of the fatigue specimens, micro-hardness tests were conducted on the base metal and heat affected zone (HAZ) in the vicinity of the weld. To perform these measurements, two untested specimens, one as-welded and one needle peened, were sectioned and the resulting samples cast in epoxy. The samples were then polished in accordance with [23] and the hardness tests were performed using a Vickers micro-hardness tester with an applied force of $P = 200$ g.

To study the microstructure of the treated weld toe, after performing the micro-hardness measurements, the surface of the

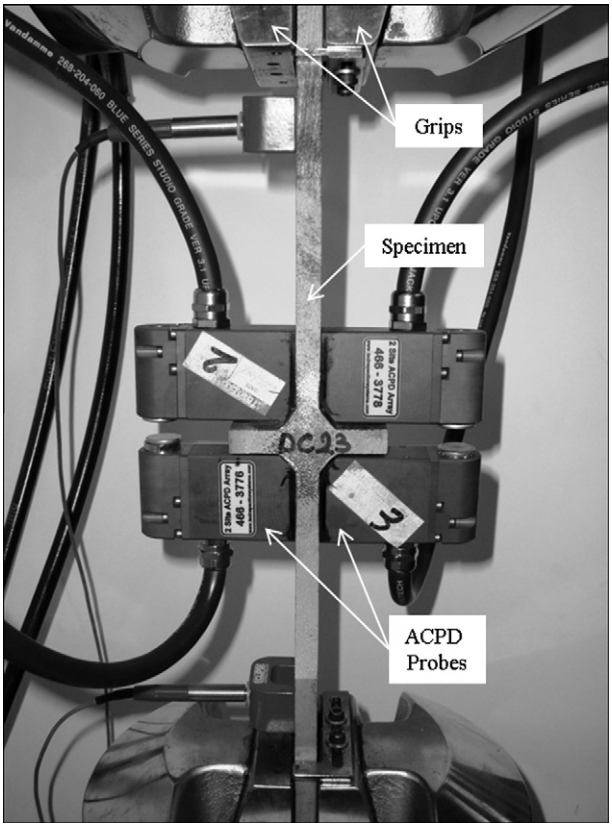

Fig. 5. Fatigue specimen in test frame with ACPD probes installed.

treated weld sample was etched with a 2% Nital solution to reveal the microstructure. Photos were then taken through a microscope at 10× magnification.

The near-surface residual stresses in the as-welded and peened welds along the anticipated crack path were measured by X-ray diffraction. These residual stress measurements were performed by Proto Manufacturing Ltd. in accordance with [24,25]. Measurements were taken at two locations on three specimens, one as-welded, one peened, and one peened and then cyclically loaded for over 3 million cycles under CA-UL loading at $\Delta S_{eq} = 186$ MPa. Along with surface measurements, subsurface measurements at nominal depths of 0.1, 0.2, 0.5, 1.0, 1.5, and 1.8 mm were obtained, using a process of electropolishing.

2.3. Weld toe geometry measurements

Weld toe angle (θ_w) and radius (ρ) measurements were obtained using photos of saw-cut weld sections. Specifically, three as-welded specimens, two untested and one cracked, and three peened specimens, two untested and one cracked, were cut into half and then polished. Photos were then taken of the weld toes and used to measure the weld toe angle and radius. Thirty-six as-welded and 36 needle peened weld toe locations were polished and photographed in total. The weld toe angle was defined as the angle between the extension of the parent plate surface and the line representing the shape of the weld near the toe area. Herein, as in [26], the weld toe radius was defined as the radius of the largest circle that can be fitted to the transition between the parent plate and the weld metal.

2.4. Cyclic and static materials tests

Static tension and cyclic tests were conducted on coupon specimens of the CSA 350 W structural steel base metal to determine

the static (E, σ_y, σ_u) and cyclic (K', n') material properties required as input for the SBFM analysis. Five flat, 9.5 mm (3/8″) thick static tension coupons were fabricated in accordance with [19]. The cyclic tests were performed on polished smooth cylindrical, variable width specimens having a 5.0 mm diameter within the 7.6 mm (0.3″) gauge length.

3. Laboratory test results

3.1. Fatigue life and crack growth behaviour

The S–N results of the fatigue tests conducted under CA loading conditions are summarized in Fig. 6a. Comparing the as-welded and needle peened results in this figure, it can be seen that in all cases, needle peening resulted in a substantial fatigue life increase. At the lower nominal stress range (180 MPa), it can be seen that increasing the stress ratio, R, from 0.1 to 0.4 resulted in a slight decrease in the fatigue lives of the untreated welds. In the case of the needle peened welds, all of the tests at $R = 0.1$ were runouts, whereas failures were observed between 1 and 2 million cycles for all of the tests performed at $R = 0.4$. In the case of the specimens tested at $R = -1.0$, even though the nominal stress range was high (400 MPa), no fatigue failures were observed in the peened welds. Several failures were observed in the grips, however, limiting the durations of these tests.

The S–N results of the tests conducted under CA-UL and VA loading are summarized in Fig. 6b. In order to facilitate the plotting and comparison of these results, an equivalent nominal stress range, ΔS_{eq}, is employed, based on Miner's sum, with a constant S–N curve slope of $m = 3.0$, in accordance with [16,17]:

$$\Delta S_{eq} = \left(\frac{\sum_{i=1}^{n} N_i \cdot \Delta S_i^3}{N_{total}} \right)^{1/3} \quad (1)$$

In Fig. 6b, it can be seen that, once again, needle peening resulted in a fatigue life increase in all cases. Comparing the two VA loading histories, it can be seen that the fatigue lives of the as-welded specimens are slightly higher on average under the ps-r-15 history. On the other hand, while all of the needle peened specimen tests were runouts under the ps-m-40 history, one fatigue failure was observed for a needle peened specimen under the ps-r-15 loading history.

In Fig. 6, S–N curves are plotted for Detail Categories 'B' and 'C' according to [16,17]. Comparing the Detail Category 'C' S–N curve to the test data, it can be seen that the fatigue lives of the untreated welds fall slightly below the design curve in some cases. In the case of the needle peened specimens, all of the test results under CA loading fall on or above the Detail Category 'B' S–N curve. Under CA-UL loading, several data points fall below this curve, but remain above the Detail Category 'C' curve. All of the test results of needle peened welds under VA loading fall above the Detail Category 'B' curve.

Fig. 7 summarizes the crack growth data acquired during fatigue testing, using the ACPD system described in Section 2.1. Crack growth curves are presented for specimens subjected to the following loading conditions: CA loading at $\Delta S = 270$ MPa ($R = 0.1$), ps-m-40 loading, and ps-r-15 loading. The curves in this figure are based on the deepest measured crack depth. Since crack depths were measured at two locations only on each weld toe, it is possible that the actual maximum crack depths were greater than these curves indicate. Nevertheless, important trends can still be identified by examining these curves. Looking at the total fatigue life curves in Fig. 7, it can be seen that needle peening delays the crack growth at the smaller crack depths. To further demonstrate this, crack growth curves considering only the number of cycles after the crack depth, a, exceeds 1.0 mm are also shown in Fig. 7a and c. Comparing the as-welded and needle peened specimen curves, it can be seen that, even though the fatigue lives of the peened specimens are considerably greater, the crack growth curves beyond 1.0 mm are similar, regardless of whether or not the specimen was peened.

At the visible crack depths, efforts were made to characterize the crack shape evolution versus crack depth. Various means were employed, including: visual inspection, dye penetrant staining, and (on additional fatigue specimens not considered part of the main study) beach marking. Based on this work, it was determined that, in the case of the as-welded specimens, crack coalescence generally occurred rapidly, and in most cases, the fatigue crack was effectively a through crack by the time it reached a depth of ~1.0 mm. In the case of the peened specimens, crack growth along the weld toe was inhibited by the compressive residual surface stresses, resulting in the observation of semi-elliptical cracks with higher aspect ratios throughout the visible crack depth range.

3.2. Micro-hardness and residual stress distributions

The results of the micro-hardness measurement study are summarized on Fig. 8a. In this figure, the average measured Vickers Hardnesses based on three measurements taken at various depths below the surface are plotted for the base metal and along the anticipated crack path for an untreated and a needle peened weld. Looking at this figure, it can be seen that the hardness distributions

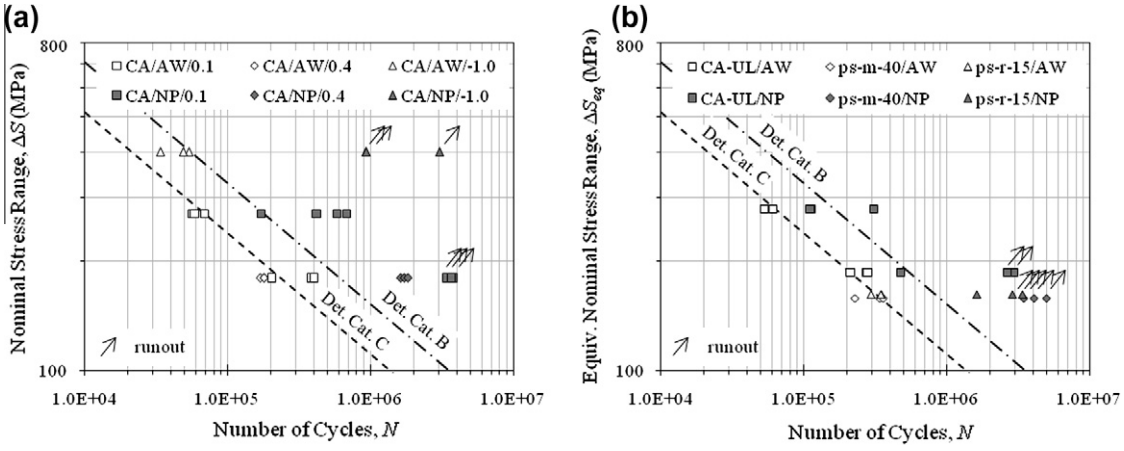

Fig. 6. Fatigue test results. (a) CA loading. (b) CA-UL and VA loading.

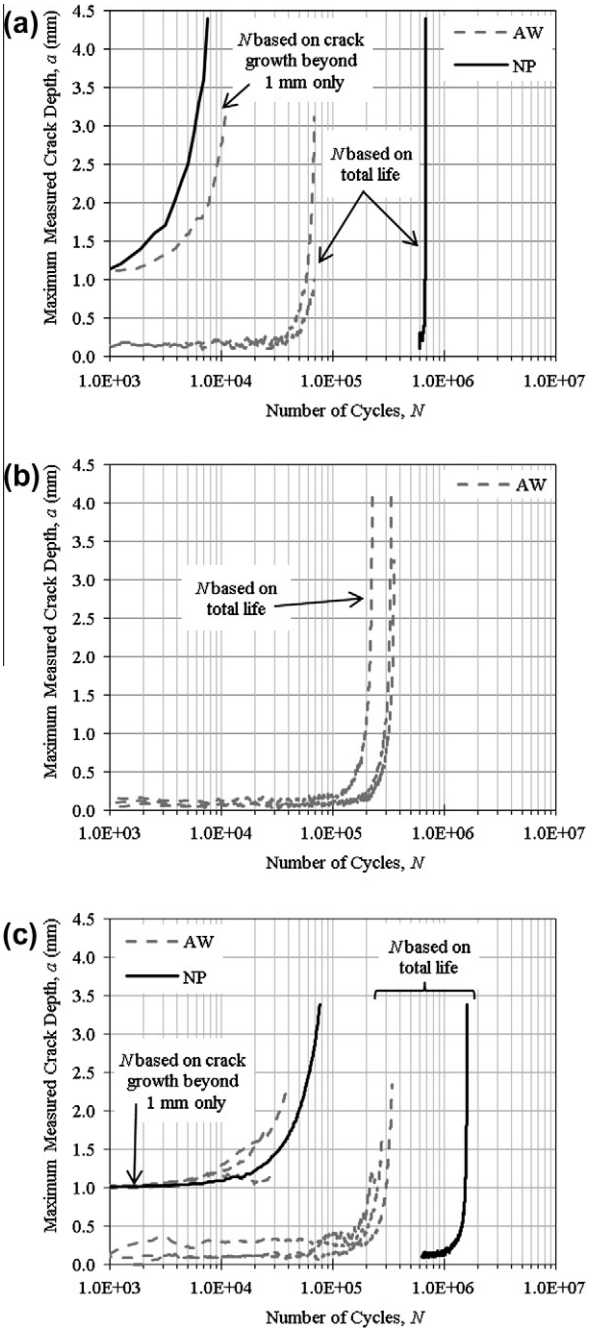

Fig. 7. ACPD crack growth measurement results. (a) CA loading at $\Delta S = 270$ MPa, $R = 0.1$. (b) ps-m-40 loading. (c) ps-r-15 loading.

for the base metal and untreated weld are relatively constant; the hardness measurements for the latter, which pass through the heat affected zone (HAZ) of the weld, are slightly higher. In Fig. 8a, it can be seen that needle peening results in a considerable increase in the near-surface hardness. The hardness decreases rapidly below the surface, however, down to the hardness of the as-welded HAZ at a depth of ~0.6 mm. Fig. 8b shows an image of the near surface microstructure of a needle peened weld. The compressed region near the needle peened surface is apparent in this figure.

The measured residual stresses for the three different specimen types discussed in Section 2.2 are summarized in Fig. 9. These measurements show an almost uniformly distributed tensile residual stress near the surface of the untreated specimen. Needle peening results in a significant change in the residual stress distribution through much of the ~1.8 mm measured depth. Near the treated surface, the residual stresses are seen to be compressive and reaching magnitudes exceeding the nominal yield strength of the material. These stresses increase gradually and approach the tensile residual stress due to welding at a depth of approximately 1 mm below the treated surface.

The peened specimen subjected to fatigue loading showed no relaxation of the compressive residuals stresses. In fact, these stresses were measured to be slightly higher in magnitude on average in this specimen. This trend is thought to be due to the inherent variability of the stresses, however, and not the fact that this specimen had been subjected to loading after it was peened.

3.3. Weld toe geometry measurements

The measured weld toe geometry parameters are summarized in Table 2. Based on these results, it can be concluded that the effect of needle peening on the weld toe geometry is very small. The differences in the mean and minimum weld toe radius measurements are insignificant. The weld toe angle decreases slightly as a result of the needle peening. This result may be due, however, to the employed angle definition. If a longer length were used to determine the line representing the weld shape, it is likely that needle peening would be seen to have no influence on the weld toe angle.

3.4. Cyclic and static material behaviour

The average static material properties of the CSA 350 W base metal determined from five tension coupon tests are as follows: $\sigma_y = 396.3$ MPa, $\sigma_u = 574.3$ MPa, $E = 201.6$ GPa. The Ramberg–Osgood cyclic material constants were determined to be: $K' = 1153.8$ MPa, and $n' = 0.165$.

4. Fracture mechanics analysis of as-received and peened welds

4.1. Description of strain-based fracture mechanics (SBFM) model

The SBFM model employed in the current study is essentially an LEFM model that has been adapted to account for non-linear material effects based on [27–30]. Fatigue life is calculated using the Paris–Erdogan crack growth law, modified to consider crack closure effects and a threshold stress intensity factor (SIF) range, ΔK_{th}, and integrated over a crack depth range, a_i to a_c:

$$N = \int_{a_i}^{a_c} \frac{da}{C \cdot \mathrm{MAX}\left(\Delta K_{eff}^m - \Delta K_{th}^m, 0\right)} \tag{2}$$

C and m in (2) are material constants, referred to subsequently herein as the "Paris constants". This integration is performed numerically. The effective stress intensity factor range, ΔK_{eff}, considering crack closure effects, is determined using the following expression:

$$\Delta K_{eff} = K_{max} - \mathrm{MAX}(K_{op}, K_{min}) \tag{3}$$

where K_{max} and K_{min} are the SIFs at the maximum and minimum levels for a given applied load cycle and K_{op} is the SIF corresponding with the crack opening stress level for that cycle. According to the SBFM model, the following expression is used to calculate each SIF:

$$K = Y \cdot E \cdot \varepsilon \cdot \sqrt{\pi \cdot a} \tag{4}$$

where ε is the local strain at depth, a, below the surface and Y is a correction factor to account for the crack shape, the free surface on one side of the crack, and the finite thickness of the cracked plate. In [12], a constant term, a_0, is added to the crack depth, a, to account for small crack effects. In the current study, this constant is ignored, as a simplification and due to the fact that its effect is

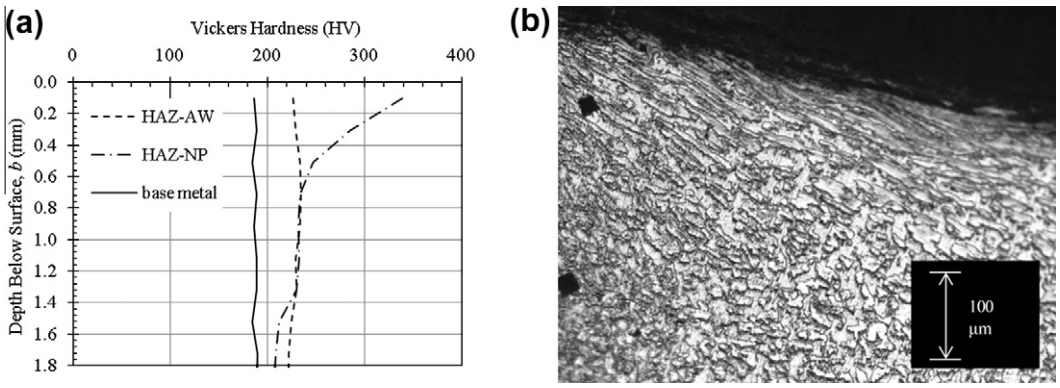

Fig. 8. Microhardness measurements and microstructure. (a) Micro-hardness measurements. (b) Microstructure near surface of needle peened weld.

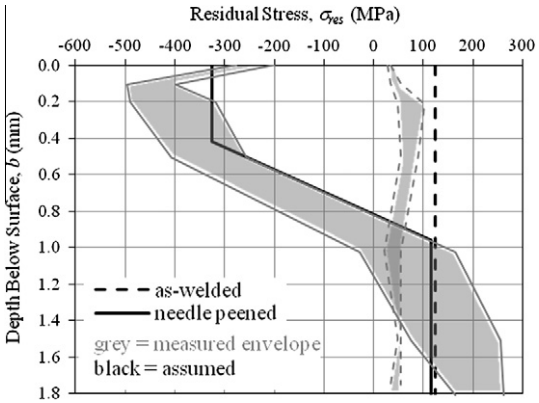

Fig. 9. Measured residual stress distributions.

Table 2
Weld toe geometry measurement results.

	As-welded		Needle peened	
	Angle (°)	Radius (mm)	Angle (°)	Radius (mm)
Max	56.0	1.25	50.0	2.09
Min	26.0	0.21	14.0	0.17
μ	39.8	0.65	29.0	0.68
σ	6.9	0.30	9.6	0.40

negligible if the initial crack depth, a_i, is as large as the one assumed herein (0.15 mm).

To calculate the stresses and strains for each load cycle, a cyclic Ramberg–Osgood material model is used [31], which requires as input the material constants: K' and n'. Strain histories at various depths below the surface of the weld notch are determined using Neuber's rule [31].

Crack closure is modelled using formulas proposed by Newman [32]. These require as input: the maximum stress level, σ_{max}, the stress ratio, R, the flow stress, σ_0 (which may be taken as the average of the yield and ultimate strength), and the plastic constraint factor, α. The plastic constraint factor is estimated based on [33]. The ratio, σ_{max}/σ_0, is modified by the correction factor, Y, as suggested in [34] and a limit on $Y \cdot \sigma_{max}/\sigma_0$ of 1.0 is introduced.

Under VA loading, along with this "steady state" crack closure model, a model for the evolution of the crack opening stress following overload events is required. For the current study, a model from [28] is employed, wherein σ_{op} is calculated using the following expression:

$$\sigma_{op} = \sigma_{cu} + \mu \cdot (\sigma_{ss} - \sigma_{cu}) \tag{5}$$

where σ_{cu} is the crack opening stress prior to the current cycle, σ_{ss} is the crack opening stress at steady state (i.e. if the crack is cycled under CA loading at the current stress range) and μ is a material constant. It has been found that $\mu = 0.002$ for SAE 1045 steel [28].

The analysis consists of cyclically loading the material at various depths below the surface of the weld notch to determine the strain parameters for each completed cycle (see Fig. 10). At any point in the load history, the local elastic stress, σ_{el}, is a function of the local elastic residual stress, $\sigma_{el,res}$, due to welding and/or peening and the local elastic stress, $\sigma_{el,app}$, due to the applied load.

Herein, the local elastic stresses are calculated using a stress concentration factor (SCF), k_p, which accounts for the presence of a crack in the weld toe, using the approach described in [30], i.e.:

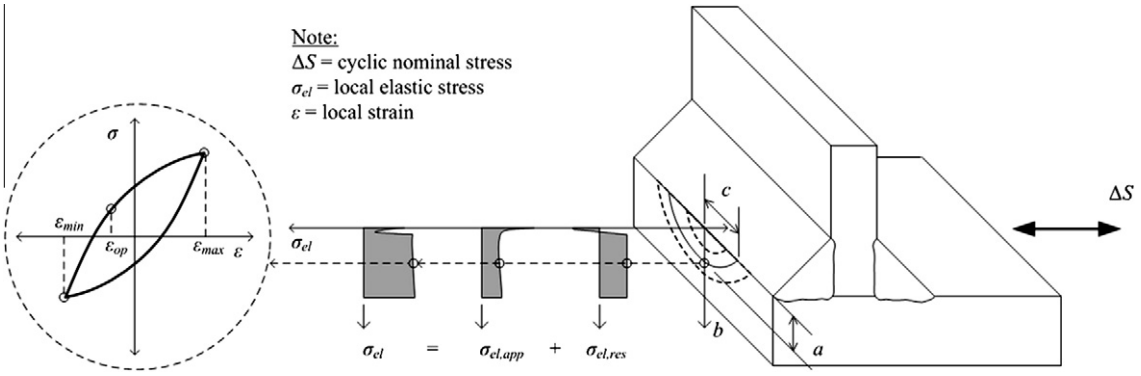

Fig. 10. Explanation of stress–strain analysis according to SBFM model.

$$k_p = \frac{K_{el}}{Y \cdot \sqrt{\pi \cdot a}} \tag{6}$$

K_{el} in this expression is the elastic SIF, accounting for the non-uniform stress distribution along the crack path. It is calculated herein using weight functions, $m(b, a, c)$, from [35], i.e.:

$$K_{el} = \int_0^a k_{el} \cdot m(b, a, c) \cdot db \tag{7}$$

where b is the depth below the surface and k_{el} is the SCF ($=\sigma_{el}/S$) for the uncracked weld toe. The local elastic stress associated with a given nominal stress level, S, is then calculated as follows:

$$\sigma_{el} = k_p \cdot S \tag{8}$$

Given the nominal stress history, the local non-linear stress–strain history is calculated. Each time a stress–strain hysteresis loop is closed, the maximum, minimum, and crack opening local strains are calculated. ΔK_{eff} is then determined and the fatigue life is calculated using (2).

A significant simplification made in the current study in the implementation of this model is that the local residual stress can be introduced by shifting the stress monotonically from zero to the specified residual stress level. In actuality, it is known that the peening stress is the result of a large plastic deformation followed by an elastic rebound (see Fig. 1a). Ignoring this means conservatively ignoring the effect of any strain hardening introduced by the peening treatment.

The described SBFM model can be employed, with a few additional rules, to perform analyses under in-service or random rather than block VA loading histories, where the definition of an overload event (tensile or compressive) is not obvious. Under such conditions, the build-up of the crack opening stress, σ_{op}, following overload events is modelled using (5). As was done in [28] based on laboratory observations (consistent with similar observations reported by others, i.e. [36]), it is assumed that if σ_{ss} for a given cycle is less than σ_{cu}, then σ_{op} immediately drops to the lower level. If σ_{ss} is greater than σ_{cu}, then (5) is employed to model the build-up of σ_{op} following the overload event. Two exceptions to these rules are: if the maximum stress level in the cycle is negative, or if the cyclic stress intensity factor range, ΔK, is less than ΔK_{th}, then it is assumed that the cycle causes no change in σ_{op}.

4.2. Input parameter assumptions

In order to implement the SBFM model, laboratory test results were used, where possible, to establish values for the various input parameters. Specifically, the elastic modulus, E, static yield and ultimate strength, σ_y and σ_u, the Ramberg–Osgood material constants, K' and n', and the weld toe geometry parameters, θ_w and ρ, were established based on the test results reported in Section 3.

In the case of the material parameters, the average base metal values reported in Section 3.4 were used. In the case of the weld toe geometry parameters, round values slightly more severe than the mean measured values were assumed ($\theta_w = 45°$ and $\rho = 0.5$ mm).

Two approaches were considered for determining k_{el} due to the applied load. In [12], this parameter was calculated using parametric equations from [37] for T-butt welds. In Fig. 11, the resulting k_{el} distribution for the 9.5 mm thick specimen is compared with a similar distribution determined by 2D (plane strain) finite element analysis (FEA) using the program ABAQUS 6.7.4 [38]. To obtain this k_{el} distribution, the uncracked specimen geometry was first analyzed to determine the location of the peak surface stress perpendicular to the loading direction. The mesh was then regenerated with a line of nodes placed perpendicular to the loading direction and passing through the peak surface stress point. In Fig. 11, it can be seen that the k_{el} distributions determined using the two methods are in close agreement. In subsequent analytical work, the FEA-based k_{el} distribution was used exclusively.

The residual stress (σ_{res}) distributions assumed in the SBFM analysis are plotted in Fig. 9 along with the corresponding measured data. For the untreated weld, a simple uniform, tensile distribution was assumed. For the needle peened weld, a three-line model was assumed.

Other input parameters assumed in the SBFM analysis are as follows: initial crack depth, $a_i = 0.15$ mm, Paris m constant = 3.0, threshold SIF range, $\Delta K_{th} = 80$ MPa $\sqrt{\text{mm}}$, critical crack depth,

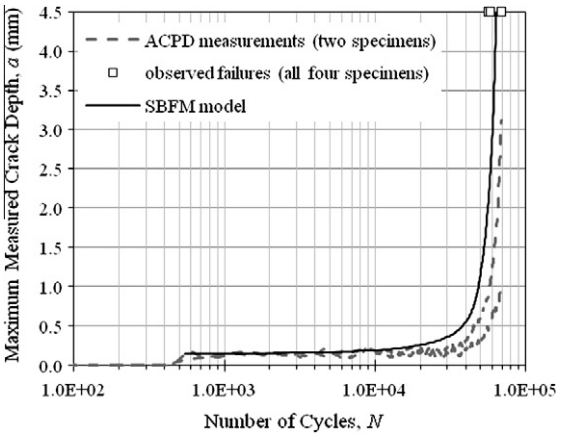

Fig. 12. Measured and predicted crack growth rates: $\Delta S = 270$ MPa, $R = 1.0$, as-welded.

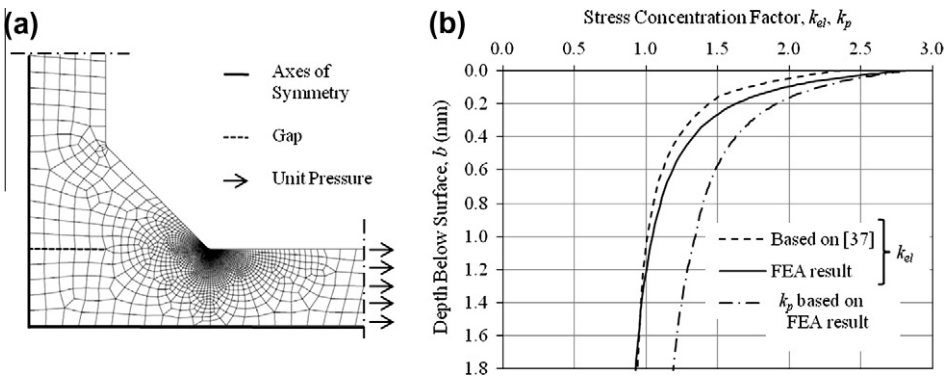

Fig. 11. Determination of SCFs. (a) FE model of weld detail. (b) SCF distribution comparison.

$a_c = 0.5 \cdot T$ (note: T = plate thickness), and $\mu = 0.002$. The assumed values for a_i, m, and ΔK_{th} are representative of the mean values for structural steel welds based on measurements reported by others. Further justification of these parameter choices is given in [12].

Given the values established for all of the other input parameters, values for the Paris C constant and crack shape versus depth function were established based on visual observation of the crack shape and fitting with the ACPD-based crack growth curves. Specifically, a value for the Paris C constant of 2.8×10^{-13} (N, mm) was established so that the model gave close predictions of the crack growth curves obtained for the untreated welds under CA loading at $\Delta S = 270$ MPa and $R = 0.1$ within the 1.0 mm < a < 3.0 mm range. Over this range, a through crack was assumed, based on the observations for this specimen type. An initial crack aspect ratio, $(a/c)_i$, of 0.6 was then fixed and the ratio, a/c, was assumed to vary linearly from 0.6 to 0.0 at a crack depth of 1.0 mm. This resulted in close fatigue life predictions for this specimen type. Although higher crack aspect ratios were observed for a > 1.0 mm in the peened specimens, this trend was conservatively ignored in the analysis.

4.3. Comparison of specimen fatigue lives and analysis predictions

In Fig. 12, the resulting SBFM model predictions are compared with the fatigue lives and ACPD-based crack growth curves for the untreated welds under CA loading at $\Delta S = 270$ MPa and $R = 0.1$. Looking at this figure, it can be seen that the shape of the crack growth curve and the average fatigue life for this specimen type are closely predicted by the SBFM model.

Fig. 13 shows a comparison of the model predictions and test results for the CA loading tests. Looking at this figure, it can be seen that the model closely predicts the applied stress ratio effects on the fatigue lives of the untreated welds. For the treated welds, at $\Delta S = 180$ MPa, the model correctly predicts finite fatigue lives for the treated welds at $R = 0.4$ and runouts for the treated welds at $R = 0.1$. The mean fatigue lives for each test type are also in close agreement. In some cases, however, the average fatigue lives of the treated welds are underpredicted slightly.

A similar comparison of for the CA-UL and VA loading tests is presented in Fig. 14. Again, the model predicts a number of significant trends observed in the test data. Specifically, it is predicted that the ps-r-15 VA loading history should result in fatigue lives greater than those under the ps-m-40 history for the untreated welds, while the reverse trend is correctly predicted for the treated welds. Again, the mean fatigue lives are also in reasonably close agreement.

5. In-service variable amplitude loading studies

5.1. Analysis under other in-service loading histories

Looking at Fig. 14, it is apparent that the degree to which the needle peening treatment increases the fatigue performance of

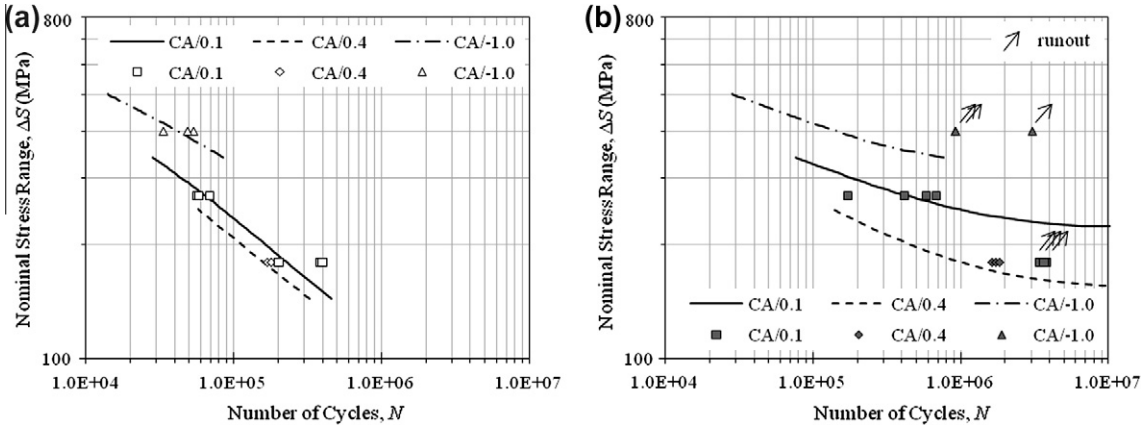

Fig. 13. SBFM results for CA loading. (a) As-welded. (b) Needle peened.

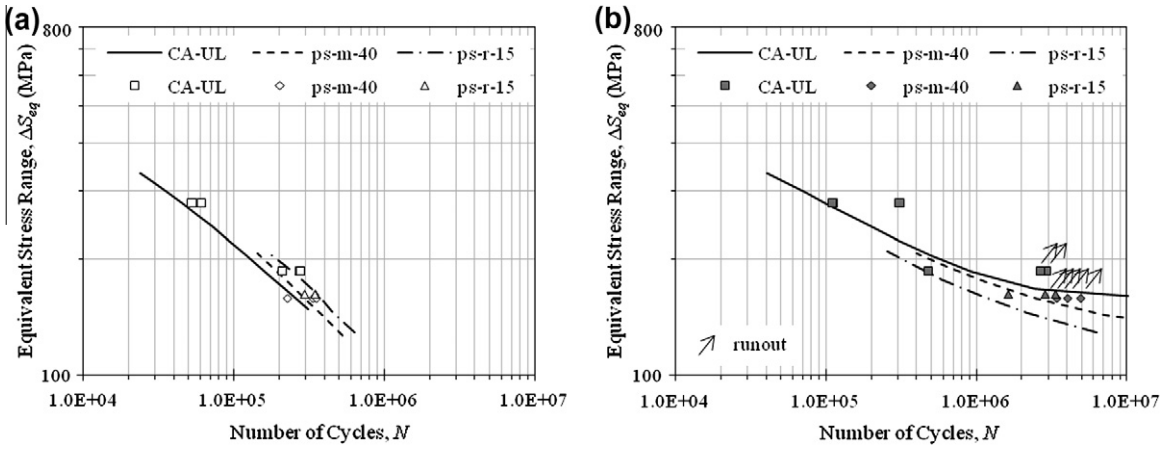

Fig. 14. SBFM results for CA-UL and VA loading. (a) As-welded. (b) Needle peened.

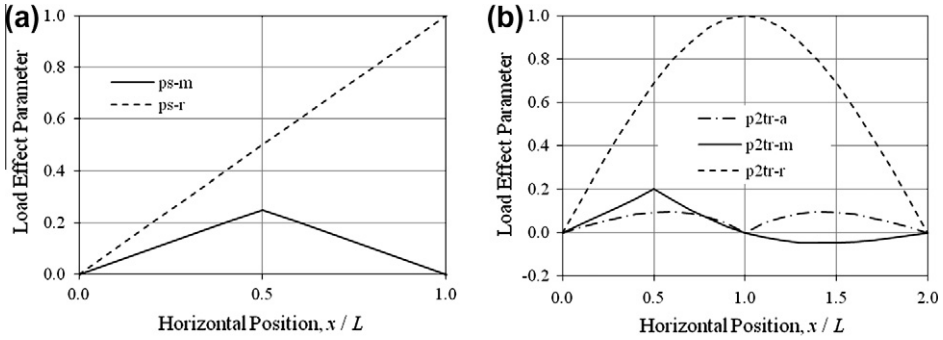

Fig. 15. Examined influence lines. (a) 1-Span simply supported girders. (b) 2-Span continuous girders.

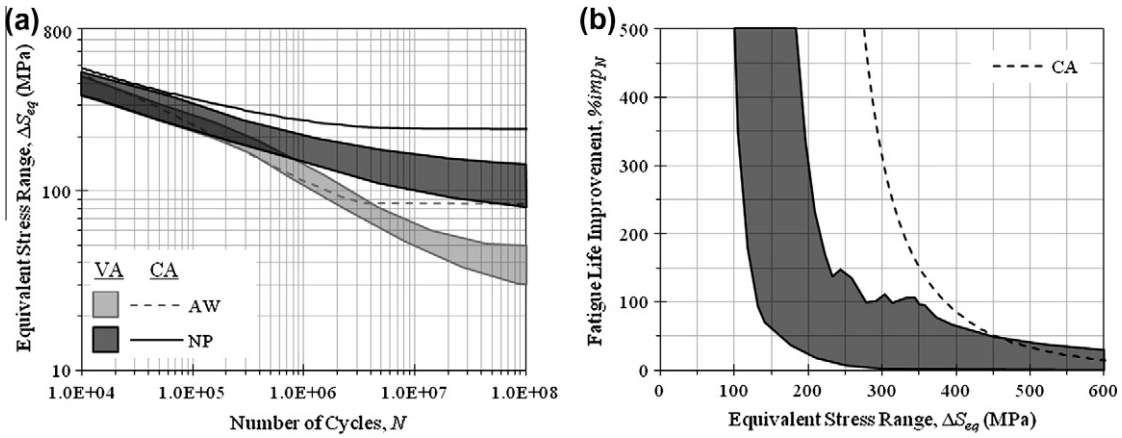

Fig. 16. Analysis results for various influence lines and bridge spans. (a) *S–N* curve envelopes. (b) Fatigue life improvement envelope.

the treated weld depends to a significant extent on the nature of the in-service loading history. Thus, in order to extend the results of the limited testing program performed for the current study to other loading histories typical of highway bridges, additional analyses were performed for a wider range of influence lines and bridge spans.

Specifically, influence lines for the following five locations were considered (see Fig. 15): mid-span moment for 1- and 2-span girders (ps-m, p2tr-m), intermediate support moment for 2-span girders (p2tr-a), and support reactions for 1- and 2-span girders (ps-r and p2tr-r). In addition, the following four bridge spans were considered: 15, 25, 40, and 60 m. The selected bridge influence lines and spans were not intended to reflect the most likely cases for fatigue cracking in highway bridges, but rather to cover a broad range of load history characteristics that can expected in these structures. To generate each loading history, a random sample of 1000 trucks taken from the 1995 Ontario survey [20] was passed over each influence line/bridge span combination.

In Fig. 16a *S–N* curve envelopes of the analysis results are presented. For comparison purposes, corresponding *S–N* curves for CA loading at $R = 0.1$ are also shown. Looking at this figure, it can be seen that the VA loading envelopes are reasonably close to the CA loading curves at the higher equivalent stress ranges, but extend below the constant amplitude fatigue limit (CAFL) at the

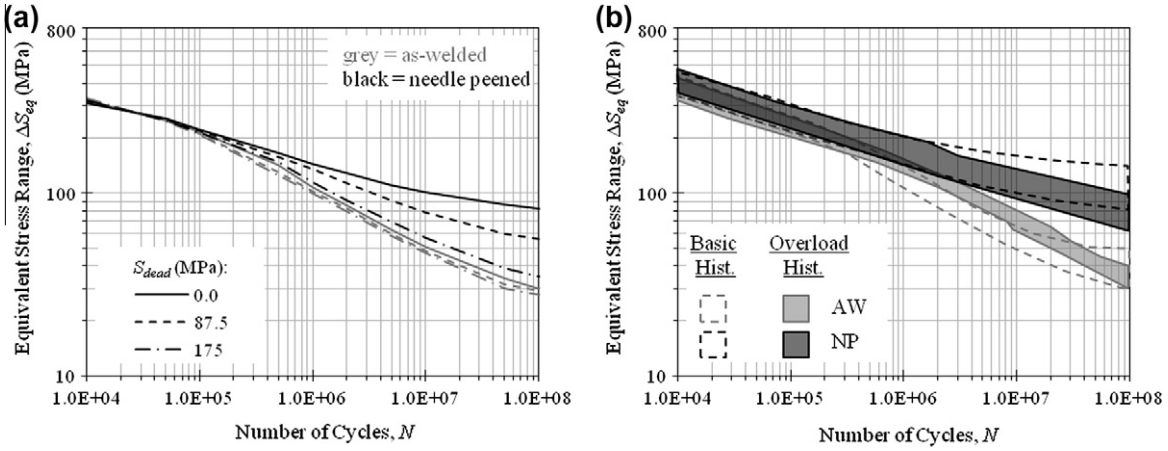

Fig. 17. Analysis results for examined dead load and overload scenarios. (a) Dead load study results. (b) Overload study results.

lower equivalent stress ranges. Under VA loading, the envelopes for the untreated and needle peened welds overlap at the higher stress ranges. This is due in part to the fact that the untreated welds are performing better under VA loading in some cases than predicted based on the CA loading analysis results. The VA loading envelope for the needle peened welds indicates that, for all of the examined cases, these welds have lower fatigue lives than predicted, given the CA loading analysis results at $R = 0.1$ and assumed definition for ΔS_{eq} (1).

In Fig. 16b the results are presented in terms of a fatigue life improvement, $\%imp_N$, envelope for the same five influence lines and four bridge spans, where:

$$\%imp = 100\% \cdot \frac{(treated - untreated)}{untreated} \quad (9)$$

Again, a curve for CA loading at $R = 0.1$ is provided for comparison purposes. Looking at this figure, it can be seen that while the envelope for the various examined VA loading histories falls below the CA loading curve, substantial fatigue life improvements are still predicted. For example, for $\Delta S_{eq} \leqslant 125$ MPa, $\%imp_N$ is greater than or equal to 100%, regardless of the load history.

5.2. Effect of dead load stresses

It has been shown by others and can also be seen in the test results reported in the current study (see Fig. 13b) that the effectiveness of peening decreases as the stress ratio increases. Since welds in bridges generally support some constant stress level (in addition to the cyclic nominal stress) due to the dead load (i.e. self weight of superstructure, road surface, etc.), additional analyses were performed with two tensile dead load stress levels assumed: 25% and 50% of the nominal yield stress of 350 MPa. The results of these additional analyses are summarized in Fig. 17a.

In Fig. 17a, only the lower bounds of the envelopes for the various influence lines and bridge spans are shown. Looking at this figure, it can be seen that the dead load stress has a negligible effect on the predicted fatigue life of the untreated weld. The fatigue life of the treated weld decreases significantly, however, as the tensile dead load stress increases, until at $S_{dead} = 175$ MPa, the effect of the needle peening treatment is only a marginal increase in fatigue performance.

5.3. Effect of periodic overload events

One concern that has been raised with the use of residual stress-based post-weld treatments such as needle peening for bridge applications is that the residual stresses introduced by the treatment may be dissipated by periodic overload events. It is believed that the SBFM model described herein is particularly well suited for investigating the significance of this problem. To demonstrate this, additional analyses are presented in this section wherein the loading history has been modified by introducing a single overload truck that reoccurs every 1000 cycles. The CL-625 (5 axle, 62.5 tonne) code truck model from [16] is used for this purpose, with each axle load multiplied by a scaling factor of 2.0. The CL-625 truck was originally developed to represent measured extreme loading events for a range of axle spacings and axle group sizes. For static design according to [16], it is multiplied by a load factor of 1.7. Thus, it is believed that the assumed overload truck weight and frequency represent a particularly extreme case. The analysis results for this overload scenario are presented in Fig. 17b.

In Fig. 17b, the equivalent stress range, ΔS_{eq}, is based on the loading history with no overload truck. This was done to allow direct comparison of the results and assumes that: (1) the overload is infrequent enough that its effect on the cumulative fatigue damage is minor and (2) the overload event is an unexpected event that is not captured by the code-defined characteristic stress range parameter. Looking at Figure, it can be seen that the addition of the overload truck actually causes an upward shift in the envelope for the untreated welds. This trend can be explained by the positive effects that tensile overloads can have on the residual stress distribution and crack closure stress level under VA loading. In the case of the treated welds, there is little effect on the envelope at the higher equivalent stress ranges (i.e. in the low cycle domain). In the high cycle domain, however, the results show that the overload truck causes a straightening of the envelope and hence lower predicted fatigue lives. This trend can be explained by the occurrence of the two underload mechanisms described in Fig. 1. Even under this extreme overload scenario, however, a significant fatigue performance increase due to needle peening is still predicted at the lower equivalent stress ranges.

6. Discussion

It is recognized that the large scatter seen in Fig. 16 in the calculated fatigue life improvement and the underprediction of the VA loading test data for the peened welds could be the result of using an equivalent stress range based on (1). To further examine this possibility, the calculated S–N curves are replotted in Fig. 18a in terms of a modified parameter, $\Delta S_{eq,mod}$, calculated using (1), but with the assumed slope of 3.0 replaced with the actual slope in the low cycle domain, based on the CA loading S–N curves for $R = 0.1$. Slopes of 3.37 and 6.72 were calculated for the untreated and needle peened welds respectively. Looking at this

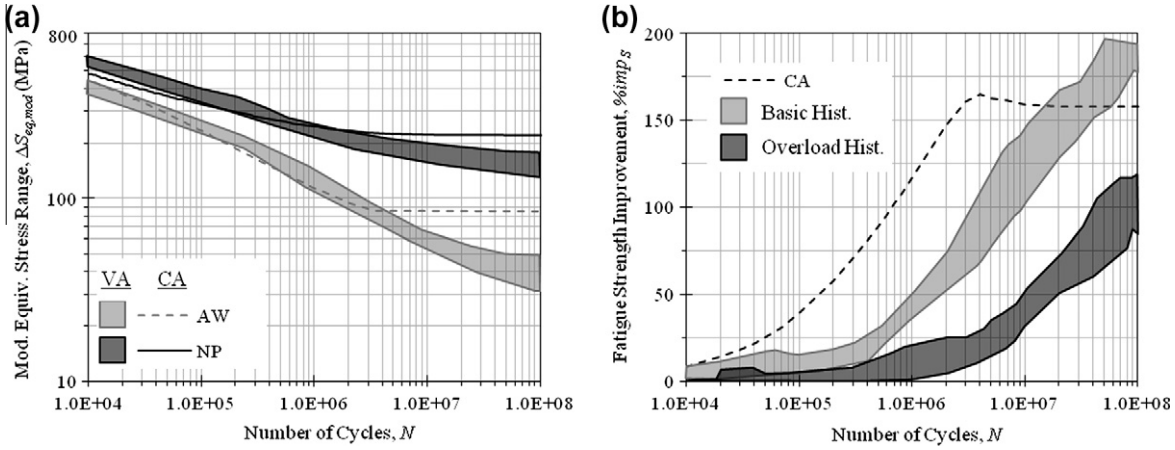

Fig. 18. Other ways of characterizing the benefit of peening. (a) Analysis results in terms of $\Delta S_{eq,mod}$. (b) Fatigue strength improvement envelopes.

figure, it can be seen that the envelopes for both cases now have a reduced width and are better aligned with the corresponding CA loading curves. Although this result represents an improvement, the consideration of varying *S–N* curve slopes in the design process may not be straight forward, since many bridge design codes (i.e. [16,17]) use effective truck models or fatigue correction factors calibrated assuming *S–N* curves for untreated steel welds, with $m = 3.0$ [39]. Furthermore, as suggested in Fig. 17a, it is possible that the *S–N* curve slopes for peened welds vary as a function of the applied stress ratio, which complicates the matter further.

One possibility that avoids these problems, suggested in [40] for UIT, is to only consider the benefit of peening in the infinite life domain. Fig. 17b shows envelopes of the fatigue strength (ΔS_{eq}) improvement, $\%imp_S$, due to needle peening for various fatigue lives. Results obtained using the basic loading history, as well as the examined overload history, are shown in this figure. Looking Fig. 17b, it can be seen that the results for the basic load history are safely predicted in the high cycle domain by the CA loading curve. Although the results for the overload history fall somewhat below the CA loading curve, they still show a significant fatigue strength increase in the high cycle domain of $\%imp_S = 85\%$ or greater. Regarding this result, it should be noted that the overload truck weight and frequency assumed in this analysis were chosen somewhat arbitrarily to represent a particularly extreme case, with the goal of illustrating the possible effects of overloads on the fatigue performance improvement due to needle peening, as predicted by the SBFM model. If this approach were to be used to develop a design code procedure, further work would be needed to select in a more rigorous way a suitable set of overload magnitudes and frequencies to be assumed in the procedure calibration.

7. Conclusions

Based on the testing and analysis results presented herein, the following conclusions are drawn:

- Needle peening introduces compressive residual stresses and increases the hardness near the surface of the treated weld toe. Its effect on the fatigue behaviour of structural steel welds is a significant increase in fatigue life under loading conditions typical of highway bridges.
- The influence of needle peening on the fatigue performance of highway bridge welds under in-service variable amplitude (VA) loading conditions can be predicted using a strain-based fracture mechanics (SBFM) model wherein the effect of the treatment is modelled as a change in the residual stress distribution along the crack path. The SBFM model is particularly well-suited for application to this problem as it implicitly considers two mechanisms that can cause peened welds to have a lower than expected fatigue performance under VA loading conditions.
- Application of the SBFM model to consider in-service loading histories encompassing a wider range of influence lines, bridge spans, and loading conditions shows that the predicted benefit of needle peening is highly dependent on the loading characteristics, as well as the presence of tensile dead load stresses. The consideration of periodic overload trucks in the analysis is also shown to result in a reduction in the fatigue performance of needle peened welds.
- Using the actual *S–N* curve slope in the calculation of the equivalent stress range reduces the scatter in the analysis results for the peened welds. Possible design approaches for bridge codes could employ fatigue correction factors or effective truck models calibrated for *S–N* curves with $m \neq 3.0$ or involve only considering the treatment benefit in the infinite life domain.
- Despite the complexities involved in accurately predicting the benefit of needle peening on the fatigue performance of bridge welds, this benefit is seen to be substantial for a wide range of loading conditions likely to be seen in highway bridges.

Although the presented research is limited to the investigation of needle peening, it is believed that the reported general trends are applicable to steel bridge welds subjected to any peening treatment that works primarily by introducing compressive residual stresses.

8. Recommendations for future work

It is recommended to extend the results of this study through further validation of the SBFM model considering large-scale fatigue test data. Scale effects are a concern, as the welds in full-scale structures tend to see higher tensile residual stresses due to the welding and fabrication process and higher local notch effects. In addition, as the total weld length is greater, there is an increased probability that a larger initial defect exists somewhere along the weld length.

Application of the SBFM model to other peening methods and in-service loading histories typical of other structure types are also recommended areas of future work. Although a number of simplifying assumptions are made herein regarding the various secondary effects of peening, the SBFM model could serve as a useful tool for studying these effects, including the influences on the fatigue behaviour of local changes in hardness and modifications of the weld toe geometry.

Acknowledgements

Financial support for this research provided by the National Sciences and Engineering Research Council of Canada (NSERC) and Canadian Institute of Steel Construction (CISC) is gratefully acknowledged. V. Baltazar, M. El Zeghayar, R. Morrison, and D. Hirst are thanked for their help with the laboratory testing. T. Topper and G. Glinka are thanked for their technical guidance.

References

[1] Harrison JD. Further techniques for improving the fatigue strength of welded joints. Brit Weld J 1966;11:642–7.
[2] Bremen U. Amelioration du comportement à la fatigue d'assemblages soudés: étude et modelisation de l'effet de contraintes residuelles. École Polytechnique Fédérale de Lausanne Thesis No. 787; 1989.
[3] Kirkhope KJ, Bell R, Caron L, Basu RI, Ma K-T. Weld detail fatigue life improvement techniques, part 1 review. Marine Struct 1999;12(6):447–74.
[4] Roy S, Fisher JW, Yen BT. Fatigue resistance of welded details enhanced by ultrasonic impact treatment (UIT). Int J Fatigue 2003;25:1239–47.
[5] Maddox SJ. Improving the fatigue strength of welded joints by peening. Metal Construct 1985;17:220–4.
[6] Kuhlmann U, Bergmann J, Dürr A, Thumser R, Günther H-P, Gerth U. Enhancement of the fatigue strength of welded high strength steels by application of post-weld treatment methods. Stahlbau 2005;74:358–65.
[7] Wang T, Wang D, Huo L, Zhang Y. Discussion on fatigue design of welded joints enhanced by ultrasonic peening treatment. Int J Fatigue 2009;31:644–50.
[8] Dubois V. Fatigue de détails soudés traités sous sollicitations d'amplitude variable. École Polytechnique Fédérale de Lausanne Thesis No. 1260; 1994.
[9] Manteghi S, Maddox SJ. Methods for fatigue life improvement of welded joints in medium and high strength steels. IIW Doc. XIII-2006-04; 2004.
[10] Huo L, Wang D, Zhang Y. Investigation of the fatigue behaviour of the welded joints treated by TIG dressing and ultrasonic peening under variable-amplitude load. Int J Fatigue 2005;27:95–101.
[11] Marquis G, Björk T. Variable amplitude fatigue strength of improved HSS welds. IIW Doc. XIII-2224-08; 2008.
[12] Walbridge S. Fatigue analysis of post-weld fatigue improvement treatments using a strain-based fracture mechanics model. Eng Fract Mech 2008;75:5057–71.
[13] Dowling NE. Estimation and correlation of fatigue lives for random loading. Int J Fatigue 1988;10(3):179–85.
[14] Zhang Y-H, Maddox SJ. Investigation of fatigue damage to welded joints under variable amplitude loading spectra. Int J Fatigue 2009;31(1):138–52.

[15] Albrecht P, Lenwari A. Variable-amplitude fatigue strength of structural steel bridge details: review and simplified model. J Bridge Eng 2009;14(4):226–37.
[16] CAN/CSA-S6-06: Canadian Highway Bridge Design Code. Canadian Standards Association. Mississauga; 2006.
[17] AASHTO LRFD bridge design specifications. American Association of State Highway and Transportation Officials, Washington (DC); 2008.
[18] Handbook of steel construction, 9th ed. Canadian Institute of Steel Construction, Toronto; 2006.
[19] ASTM E-8: standard test methods for tension testing of metallic materials. American Society for Testing and Materials; 2004.
[20] Ontario commercial vehicle survey. Ministry of Transportation of Ontario; 1995.
[21] Ghahremani K. Predicting the effectiveness of post-weld treatments applied under load. University of Waterloo MASc Thesis; 2010.
[22] Hobbacher A. Recommendations for fatigue design of welded joints and components. IIW Doc. XIII-1965-03/XV-1127-03; 2005.
[23] ASTM E3-01: standard guide for preparation of metallographic specimens. American Society for Testing and Materials; 2007.
[24] ASTM E915: standard test method for verifying the alignment of X-ray diffraction instrumentation for residual stress measurement. American Society for Testing and Materials; 2002.
[25] SAE HS784: residual stress measurement by X-ray diffraction. Society of Automotive Engineers International; 2003.
[26] Lopez Martinez L, Korsgren P. Characterization of initial defect distribution and weld geometry in welded fatigue test specimens. IIW Doc. XIII-WG4-60-94; 1993.
[27] Lam TS, Topper TH, Conle FA. Derivation of crack closure and crack growth rate data from effective-strain fatigue life data for fracture mechanics fatigue life predictions. Int J Fatigue 1998;20:703–10.
[28] Khalil M, Topper TH. Prediction of crack-opening stress levels for 1045 as-received steel under service loading spectra. Int J Fatigue 2003;25:149–57.
[29] ElHaddad MH, Topper TH, Smith KN. Prediction of non propagating cracks. Eng Fract Mech 1979;11:573–84.
[30] Dabayeh AA, Berube AJ, Topper TH. An experimental study of the effect of a flaw at a notch root on the fatigue life of cast Al 319. Int J Fatigue 1998;20(7):517–30.
[31] Dowling NE. Mechanical behaviour of materials. Upper Saddle River (NJ): Pearson Education Inc.; 2007.
[32] Newman JC. A crack opening stress equation for fatigue crack growth. Int J Fracture 1994;24:R131–5.
[33] Wang CH, Rose LRF, Newman JC. Closure of plane-strain cracks under large-scale yielding conditions. Fatigue Fract Eng Mater Struct 2002;25:127–39.
[34] McClung RC. Finite element analysis of specimen geometry effects on fatigue crack closure. Fatigue Fract Eng Mater Struct 1994;17:861–72.
[35] Shen G, Glinka G. Weight functions for a surface semi-elliptical crack in a finite thickness plate. Theor Appl Fract Mech 1991;15(3):247–55.
[36] Vormwald M, Seeger T. Consequences of short crack closure on fatigue crack growth under variable amplitude loading. Fatigue Fract Eng Mater Struct 1991;14:205–25.
[37] Monahan CC. Early fatigue crack growth at welds. Billerica (MA): Computational Mechanics Publications; 1995.
[38] ABAQUS 6.7.4. User documentation. Dassault Systems; 2007.
[39] Walbridge S, Coughlin R. Aluminum bridge structures – recommendations regarding design *S–N* curves and fatigue correction factor. In: 2nd International conference on fatigue and fracture in the infrastructure, Philadelphia; 2009.
[40] Roy S, Fisher JW. Modified AASHTO design *S–N* curves for post-weld treated weld details. Bridge Struct 2006;2(4):207–22.